Journal of Shipping and Ocean Engineering 16 (2026) 1-10
Doi: 10.17265/2159-5879/2026.01.001

Wave Height Detection Using Small Ship Motion Based on Detection of Three-Dimensional Center of Gravity

Yu Zhuang, Yutaka Watanabe and Kailun Yu

Graduate School of Tokyo University of Marine Science and Technology, Laboratory of Detection of Three-Dimensional Center of Gravity Inc., Tokyo 1358533, Japan

Abstract: Small ships such as fishing boats often lack reliable weather prediction systems and safety equipment, making it difficult to obtain accurate sea condition information. When wave heights exceed safe limits, ship stability decreases, thereby increasing the risk of capsizing. This study applies D3DCG (Detection of Three-Dimensional Center of Gravity) to assess wave response characteristics and to ascertain the maximum wave height small ships can withstand under different motion conditions. Ship model experiments were conducted to measure real-time wave heights under different rotational motions. Results were compared with computational predictions. The findings indicate that the wave-gauge-measured wave heights are generally greater than the calculated values, although both exhibit similar trends of variation. The maximum tolerable wave height exhibits a nonlinear pattern, indicating that ship stability varies considerably with the motion state. Overall, D3DCG reflects real-time stability changes effectively and provides a practical approach for evaluating safe operation under uncertain wave conditions, offering valuable insights for maritime safety monitoring and early warning in the absence of meteorological support.

Key words: Capsizing prevention, D3DCG, real-time wave height, small ships.

1. Introduction

Ships, including small vessels, play important roles in global shipping and fisheries industries. They are indispensable means of transportation. However, during maritime operations of ships, many factors can cause capsizing accidents, including internal factors related to the ship itself and external factors such as the environment. High sensitivity of ship capsizing to initial conditions has represented a complex research topic for decades [1-4]. For many capsizing accidents involving small ships, finding an accident cause is difficult, whether it is a calm sea surface with good weather conditions or a sea surface with bad weather conditions. In past years, the asymptotic Lyapunov exponent has been calculated from equations of motion for the mooring problem [5], single-degree-of-freedom capsize models [6-10], and works elucidating rudder angle effects while surf-riding because they address capsizing [11]. Evaluating ship capsizing accidents typically requires knowledge of a range of ship parameters and load conditions [12]. Ship capsizing prediction is often a complex process. For early research, the ship motion state was observed based on temporal changes [13]. For better protection of small vessels, especially fishing boats, yachts [14], and other small craft that do not carry expensive radar or AIS (Automatic Identification System), real-time wave height measurement is conducted based on D3DCG (Detection of Three-Dimensional Center of Gravity). The maximum wave height which a ship can withstand is calculated in real time. The actual wave height is compared with maximum wave height data to provide accurate data and other information to vessel operators and to prevent accidents from occurring.

Some small ship capsizing accidents are illustrative: On December 20, 2024, the captain of a tuna fishing

Corresponding author: Yutaka Watanabe, doctor of engineering, specially appointed professor, research fields: the center of gravity detection and transportation safety.

boat died after his vessel capsized off Oma, Aomori Prefecture, Japan [15, 16]. On January 6, 2025, in the capsizing accident of the No. 8 Hamamaru fishing boat in the waters off Kashima Port in Ibaraki Prefecture, two people died; three have remained missing [17].

Given such a background, research elucidating ship navigation safety, especially unknown wave height, has become a hot research topic. To reduce ship capsizing risk, researchers have proposed different preventive approaches after investigating the problem from various perspectives. If the roll motion characteristics of a ship during capsizing are known, then the capsizing probability can be calculated. In this way, research investigating the capsizing criteria in beam seas has been increased to elucidate characteristics of the rolling motions of capsizing ships [18]. This study assesses a method for wave height detection based on ship motion on the sea surface. Furthermore, this report describes a study of capsizing criteria under beam sea conditions to describe rolling motion characteristics of ships during capsizing more accurately, thereby giving a theoretical basis for calculating the capsizing probability.

2. Material and Methods

These analyses use ship scale models to collect data of actual sea surfaces and to collect motion data through single-turn motion using ship models. Ship motion data are received by motion sensors, which can record angles, angular velocities, and accelerations from three directions. The motion sensor sampling rate is 20 Hz. D3DCG (Detection of Three-Dimensional Center of Gravity) [19-22] is used to detect the height of the ship's center of gravity [23], and subsequently to calculate D3DCG-related parameters. Real-time water surface wave height and the maximum wave height which can be sustained in real time are calculated based on the ship's own motion state. Generally speaking, measuring specific parameters and cargo loading capacities of small vessels such as actual fishing boats is difficult. Therefore, when ship information and parameters are unknown, all data collection is based on D3DCG.

2.1 Detection of Three-Dimensional Center of Gravity (D3DCG) for the Ship

This study uses D3DCG, a method of ascertaining the center-of-gravity position based on the motion state of an object. D3DCG is derived from the ship buoyancy principle. On a calm water surface, the ship maintains vibration on the water surface. The vibration frequency depends on the distance from the motion axis to the center of gravity. Therefore, D3DCG can estimate the center of gravity by estimating the motion frequency. Ships invariably have motions of six kinds on the water surface: heave, roll, surge, pitch, sway, and yaw. The heaving and rolling motions are necessary for D3DCG. The ship movement state is portrayed in Fig. 1 as a cross-sectional view from the bow to the stern direction. As Fig. 1 shows, the motion of particles floating on the water surface generates circular motion through waves. Ships are also governed by this motion. The ship generates a single vertical vibration and a horizontal roller at its center of gravity based on a specific axis position located underwater. Waves appearing on the water surface are generated by circular motion, which diminishes and which eventually reaches zero with increasing distance from the surface. This stable point can be regarded as the fulcrum of the previously described wave motion. In other words, it is the wave motion axis. According to the new D3DCG concept, this axis also involves hull oscillation and affects ship stability to a considerable degree. Results show that the ship rolling accompanies the wave motion. The right-left swing width increases with wave height, as presented below.

$$l^2 + \frac{g}{4\pi^2 v^2} l - \frac{b^2 v'^2}{4v^2} = 0 \tag{1}$$

$$l_{max} = \frac{\pi^2 v'^2 b^2}{g} \tag{2}$$

Because of the constant position of the center of gravity inside the hull relative to the vertical direction, the restoring force of the hull can be regarded as representing the potential energy in the vertical direction, as presented in Fig. 2. If that relation exists, then the hull will not capsize. By contrast, if the hull tilts left-right, then the hull will capsize when the tilt angle exceeds a certain limit. If this extreme angle is set as θ_{max}, then the equation is the following.

$$\cos\theta_{max} = \frac{l}{l_{max}} \tag{3}$$

Equations (1), (2), and (3) are combined to obtain Equation (4) shown below.

$$\frac{16\pi^4 v^4}{g^2} l^3 + \frac{8\pi^2 v^2}{g} l^2 - \frac{v^2}{v'^2} l - \frac{g}{4\pi^2 v'^2} = 0 \tag{4}$$

Here, v represents the horizontal vibration (rolling) frequency, v' denotes the vertical vibration (heaving) frequency, l stands for the distance between the center of gravity and the axis, and l_{max} expresses the maximum height of l to remain stabilized. In the equations, θ denotes the inclination angle of the center of gravity, θ_{max} represents the maximum stable inclination angle of the center of gravity, π represents the ratio of the circumference of a circle to its diameter, g stands for gravitational acceleration, and b denotes the horizontal width which produces the restoring force.

In practice, D3DCG can evaluate the center of gravity by estimation of the restoring force. According to Fig. 2, the distance of horizontal vibration is b: when the ship's horizontal motion exceeds b, the ship will capsize. In addition, θ_{max} denotes the maximum angle of motion to be stabilized. From the perspective of the natural center of motion, if the ship tilts on the water surface, then the value of l_{max} decreases as the value of $b/2$ increases, as presented in Fig. 2. At a certain point, the values of l_{max} are equal to l. Furthermore, l_{max} of less than l corresponds to the condition for capsizing: the ship will capsize. The value of $b/2$ is obtainable using the simple mathematical equation presented above. In this case, the rolling motion resembles a simple pendulum motion. Heaving motion is a simple harmonic motion, which has a straightforward comparison in physics.

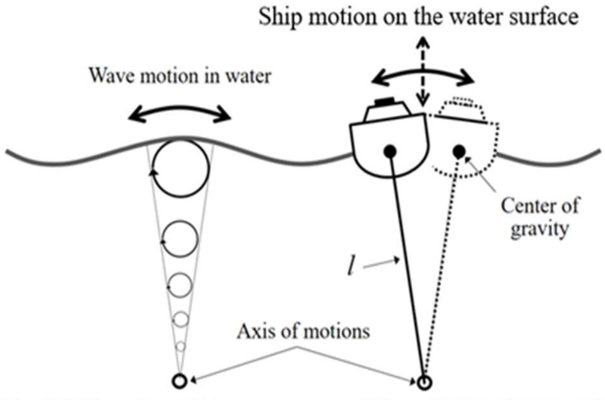

Fig. 1 Ship movement on a water surface.

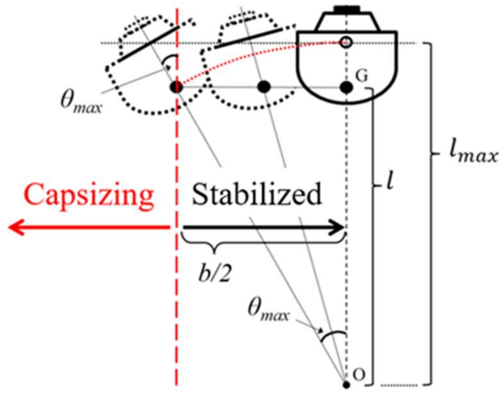

Fig. 2 Ship stability and capsizing conditions.

2.2 Wave Height and Maximum Wave Height Measurements

Regarding capsizing, it is noteworthy that the wave heights affecting each vessel differ. For instance, for a large ship, the hull tilt might become considerably large if the ship is subjected to wave heights such as long-term undulations, as depicted in Fig. 3. However, even if small ships are subjected to such long-period waves, the tilt relative to the water surface is not significant. By contrast, if subjected to short period waves little by little, then small boats might sway greatly, similarly to leaves floating on the water surface. In certain situations, however, even large vessels are subjected to such short period waves, which have almost no effect on the hull, as presented in Fig. 4.

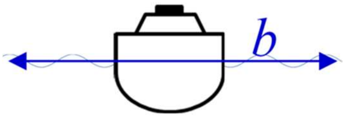

Fig. 3 Large ship tilts on a long-period wave.

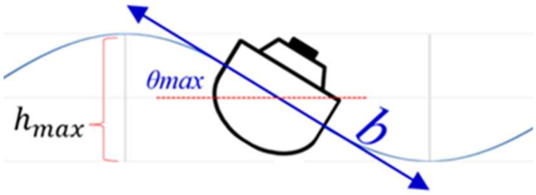

Fig. 4 Small ship tilts on a short-period wave.

The maximum wave height equation is the following.

$$h_{max} = \frac{2b}{\pi} \sin \theta_{max} \tag{5}$$

When treating waves as sine waves, the sine wave peak is lower than the linear peak by the ratio of $2/\pi$, as presented below.

$$h = h_{max} \frac{sin\theta_{rms}}{sin\theta_{max}} \tag{6}$$

Alternatively,

$$h = h_{max} \frac{\theta_{rms}}{\theta_{max}}. \tag{7}$$

2.3 Ship Scale Model Single-Turn Experiments

To verify the real-time wave height measurement of D3DCG for ships, the author conducted a series of single-turning experiments of ship scale models on actual sea surfaces (pond). Fig. 5 portrays the ship scale model used for experimentation. Normally, the yacht length is 10-13 m. The ship scale model length is about 0.33 m. Therefore, the ship scale model is about 1:33. Inside of the ship is the microcomputer with connection to a motion sensor, engine, steering engine, and weight to balance the side of the ship. In single-turn experiments, the ship angle during circling is in same degree of the rudder. Motion data are collected when changing speed.

Fig. 6 shows the wave height gauge on land. We use the gauge because the conventionally observed wave height is necessary to compare D3DCG's wave height. However, existing wave detectors are used mostly by the coast guard or weather reporting companies, which have a large range but which have a rough minimum range such as 0.5 m. This is too large a minimum for the ship scale model described in this report. Therefore, we constructed a land-fixed ultrasonic wave detector to prove that the D3DCG's wave height is meaningful for each ship. To use the wave detector, the measured distance data were converted statistically to data similar to the representative wave. The wave gauge uses either AC (alternate current) or SD (standard deviation) to represent variety of wave heights statistically in each 10 s.

Fig. 7 depicts the ship scale model control system, which is connected to the microcomputer in the ship scale model using Wi-Fi. The control panel for controlling acceleration and rudder angles is shown on the computer screen. The ship scale model is running on the water surface in the distance. This operating system can reach a signal range of 80 m through a Wi-Fi connection.

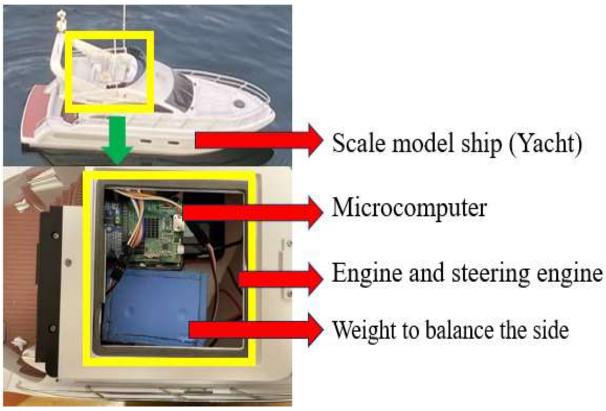

Fig. 5 Ship scale model (yacht).

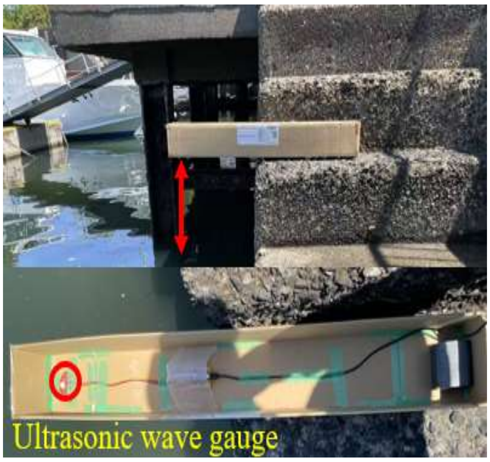

Fig. 6 Wave gauge with ultrasonic wave.

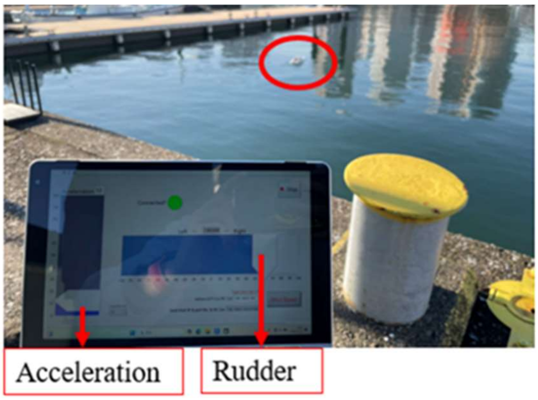

Fig. 7 Ship scale model controller.

3. Results and Discussion

3.1 Single-Turn Experiment Results

The experiments include three groups of controlled experiments with different accelerations of clockwise single turns.

Tables present results of clockwise single-turn experiments conducted at low, medium, and high acceleration, including rolling (v) and heaving (v') frequencies at different times for each experiment. By calculation based on frequency data v and v', we obtained the center of gravity height (l) and maximum center of gravity height (l_{max}) of the ship scale model, as well as the lateral vibration distance of the ship (b). In fact, l/l_{max} represents the risk of capsizing. The root-mean-square value of the ship's roll motion angle (θ_{rms}) is also provided.

For this study, after calculating h and h_{max} from the data in the table, we fill in the table with the average value of the real-time wave gauge data. Here, h is the real-time wave height on board as obtained using D3DCG (FFT size, 2048; sampling rate, 20 Hz), h_{max} denotes the real-time maximum wave height on board derived from D3DCG calculations. The following analysis introduces h_{AC} and h_{SD}: h_{AC} is the alternate current wave height observed for each 10 s by the ultrasonic wave gauge; h_{SD} is the standard deviated wave height observed each 10 s by the ultrasonic wave gauge. Hereinafter, h is an abbreviation of "real-time wave height by D3DCG"; h_{max} might be an abbreviation of "maximum wave height ship can withstand by D3DCG". In the same manner, h_{AC} might be an abbreviation of "alternated current wave height" and h_{SD} might be an abbreviation of "standard deviated wave height". These definitions of h_{AC} and h_{SD} could be regarded as the significant wave height compared with the calculated h results of D3DCG.

Table 1 Clockwise single-turn, low-acceleration experiments.

Percentage of full acceleration and time (HH:MM)	12 (14:01)	12 (14:04)	12 (14:06)	15 (14:14)	15 (14:19)	15 (14:25)	20 (14:28)
v (Hz)	1.26953	1.36719	1.48438	1.32813	1.425781	1.23047	1.28906
v' (Hz)	0.66406	0.97656	0.58593	1.40625	1.816406	1.09375	1.09375
l (m)	0.25060	0.15370	0.24920	0.10610	0.0753	0.14950	0.14330
l_{max} (m)	0.65830	0.33150	0.80060	0.18600	0.1218	0.28570	0.28060
b (m)	1.21750	0.58750	1.52170	0.30560	0.1915	0.48700	0.48260
θ_{max} (deg)	67.6254	62.3832	71.8621	55.2341	51.7988	58.4573	59.3045
h_{max} (m)	0.71670	0.33140	0.92060	0.15980	0.0958	0.26420	0.26420
θ_{rms} (deg)	0.85761	0.87998	0.87244	0.89420	0.89866	0.97727	0.96774
h (m)	0.00910	0.00470	0.01180	0.00260	0.00170	0.00440	0.00430
h_{AC} (m)	0.00928	0.01208	0.01197	0.00979	0.01697	0.01411	0.01415
h_{SD} (m)	0.00523	0.00701	0.00675	0.00549	0.00919	0.00768	0.00778
l/l_{max}	0.38068	0.46365	0.31127	0.57043	0.61823	0.52328	0.51069

Table 2 Clockwise single-turn, mid-acceleration experiments.

Percentage of full acceleration and time (HH:MM)	20 (Data lost)	25 (10:52)	30 (11:00)	35 (11:14)	40 (11:22)	45 (11:29)
v (Hz)		1.11328	1.26953	1.58203	1.23046	1.50391
v' (Hz)		0.80078	2.48047	2.22656	1.40625	1.69922
l (m)		0.23000	0.06010	0.05500	0.11380	0.07710
l_{max} (m)		0.49420	0.08360	0.08540	0.19270	0.13130
b (m)		0.87480	0.11610	0.13080	0.31100	0.21250
θ_{max} (deg)		62.2603	44.0074	49.9545	53.8164	54.0287
h_{max} (m)		0.49290	0.05140	0.06380	0.15980	0.10950
θ_{rms} (deg)		0.91540	3.10551	1.18302	0.83707	1.07708
h (m)		0.00725	0.00363	0.00151	0.00248	0.00218
h_{AC} (m)		0.02045	0.01544	0.02071	0.02021	0.03118
h_{SD} (m)		0.01134	0.00824	0.01094	0.01147	0.01823
l/l_{max}		0.46540	0.71890	0.64403	0.59056	0.58720

Table 3 Clockwise single-turn, high-acceleration change experiments.

Percentage of full acceleration and time (HH:MM)	50 (15:39)	60 (15:42)	70 (15:45)	80 (15:48)	90 (15:51)	40 (15:54)	30 (15:57)
v (Hz)	1.25000	1.50391	1.40625	1.81641	1.54297	1.38672	1.48438
v' (Hz)	1.05469	0.97656	1.91406	2.05078	2.14844	2.24609	1.97266
l (m)	0.15330	0.14100	0.07210	0.05290	0.05850	0.06150	0.06640
l_{max} (m)	0.30120	0.32200	0.11360	0.09010	0.09120	0.09090	0.10560
b (m)	0.51850	0.57900	0.17540	0.14580	0.14010	0.13370	0.16410
θ_{max} (deg)	59.4060	64.0386	50.5727	54.0425	50.1524	47.3769	51.0154
h_{max} (m)	0.28410	0.33140	0.08630	0.07520	0.06850	0.06260	0.08120
θ_{rms} (deg)	0.86816	0.74935	0.78355	1.17883	1.56769	3.15763	0.81981
h (m)	0.00415	0.00388	0.00134	0.00164	0.00214	0.00417	0.00131
h_{AC} (m)					0.01125	0.01032	0.00937
h_{SD} (m)					0.00588	0.00561	0.00512
l/l_{max}	0.50896	0.43789	0.63468	0.58713	0.64145	0.67657	0.62879

3.2 Low-Acceleration Single-Turn Experiment Results

According to Fig. 8, the overall trend shows large fluctuation amplitude, but a marked difference is apparent in the calculated h under the same 12% acceleration condition. At 14:01 and 14:06, the accelerations are both 12% of full acceleration. Also, h is consistent with h_{AC}, which indicates a certain consistency between the actual detected wave height by the wave gauge and h, but because of various factors, h is generally lower than the actual detected wave height as the acceleration increased.

Fig. 9 shows that the maximum tolerable wave height has a decreasing trend with several fluctuations during the experiment. At the beginning of the experiment, h_{max} was approximately 0.7 m. It decreased to about 0.33 m at 14:04. It then increased sharply to about 0.9 m at 14:06, which was the highest value observed. In this condition, the ship might be affected by environmental factors such as wind. After this peak, h_{max} decreased gradually. At 14:14 and 14:19, the values dropped respectively to approximately 0.15 m and 0.10 m, indicating weakened wave resistance of the ship model. Slight rebounds were observed at 14:25

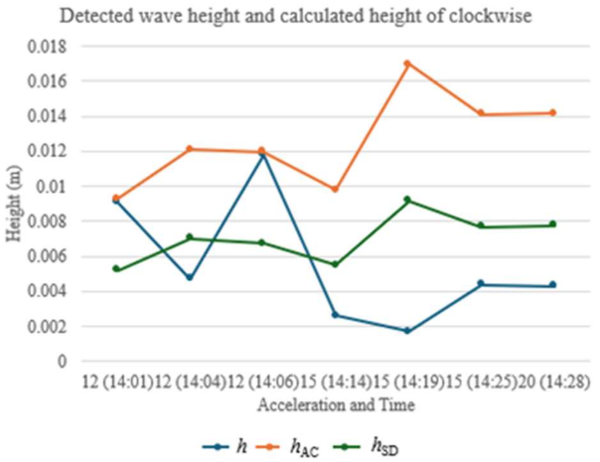

Fig. 8 Real-time wave height of low-acceleration (12%-20% of full acceleration) experiments.

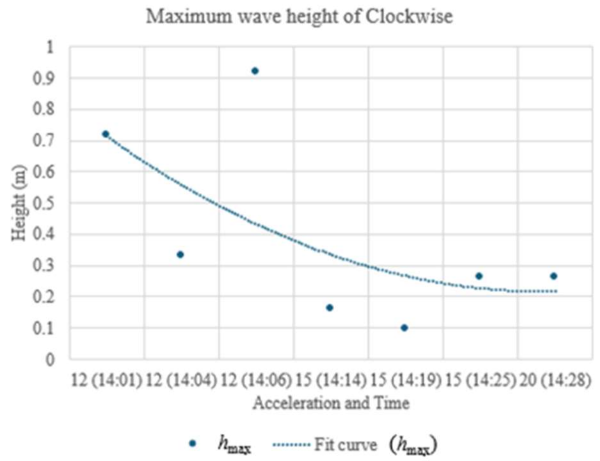

Fig. 9 Maximum wave height in low-acceleration (12%-20% of full acceleration) experiments.

14:28, with values of approximately 0.26-0.27 m, although these remained lower than the initial level. The fitting curve further shows a nonlinear downward trend that gradually stabilizes in the later stage of the experiment. Overall, the results suggest that the h_{max} which a ship can withstand decreases concomitantly with increasing acceleration, but under the same acceleration conditions, it exhibits different wave-resistance capabilities.

3.3 Mid-acceleration Single-Turn Experiment Results

From Fig. 10, it is apparent that h remained at a low level throughout the entire experiment process. Moreover, it showed a trend of first decreasing and then fluctuating slightly.

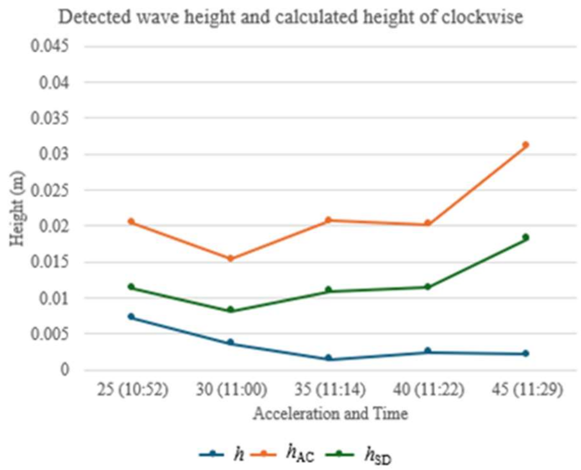

Fig. 10 Real-time wave height of mid-acceleration (25%-45% of full acceleration) experiments.

At 10:52, h was 0.007 m, and it then decreased gradually as the acceleration increased, reaching the lowest value at 11:14. Later, slight rebounds occurred at 11:22 and 11:29, but the overall value remained 0.003 m, indicating that h had slight variation of amplitude. Greater wave height showed a certain increasing trend with the experiment process, indicating that the actual wave height increased gradually with enhancement by waves created by the moving ship. However, as the acceleration increases, h shows a decreasing trend, indicating that the actual wave height borne by the ship decreases under certain conditions because of the ship speed.

Fig. 11 shows a trend of an initially strong decrease and then slight recovery. At the initial stage of the

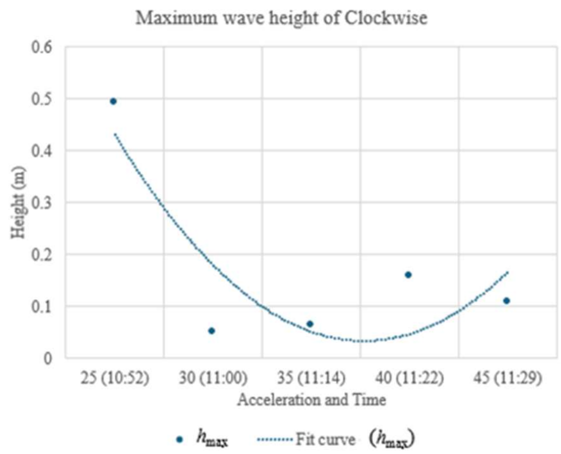

Fig. 11 Maximum wave height in mid-acceleration (25%-45% of full acceleration) experiments.

experiment, the value of h_{max} that the ship can withstand was 0.49 m: the highest value of the entire experiment process. The fitting curve in the figure shows that h_{max} exhibits a nonlinear trend with the experiment process: it decreases rapidly in the early stage; it then reaches its lowest value; thereafter, it recovers gradually. That pattern reflects that the wave resistance of the ship model first weakens and then recovers to some degree with changes in acceleration and the motion state.

The results obtained from tests of mid-acceleration suggest that the h_{max} which a ship can withstand is not entirely affected by its speed.

3.4 High-Acceleration Single-Turn Experiment Results

The wave gauge was lost between 15:39 and 15:48. It is clearly apparent from Fig. 12 that h shows a marked downward trend as the acceleration increases, reaching its lowest point at 15:45. When the acceleration decreases from 90% to 40%, h increases markedly at 15:54. Thereafter, it decreases considerably again when the acceleration decreases to 30%. The results indicate that although in open areas, the navigation waves generated by ships traveling at high speeds not only affect the wave gauge results: they also affect h. Based on this finding, it is speculated that even if the detected wave height does not present sufficient risk of capsizing a vessel when small ships are surrounded by high-speed or larger vessels, they will still capsize because of navigation waves generated by other vessels traveling at high speeds.

Fig. 13 shows the variation of h_{max} which the ship model can withstand with acceleration and time under real-time experiment conditions. The scattered data and fitting curve show that the overall trend of h_{max} exhibits a marked decrease, followed by gradual change. At the beginning of the experiment, the h_{max} which the ship model can withstand was very high, even increasing from 50% to 60% acceleration. However, from 60% to 70%, h_{max} decreased drastically, but there was no marked change during the rapid change of acceleration. Because of inertia, the actual speed does not decrease immediately, although the acceleration changes rapidly.

3.5 Discussion

The results showed that h and h_{max} might have a trend by which they decreased as the speed increased. The early results obtained for each experiment showed higher values of both h and h_{max}. By contrast, the later ones showed lower values than both, perhaps because the pond water surface was calm initially, but the waves caused by the ship scale model (sailing wave) reflected off of the pond wall and came back across the water surface around the ship scale model. The sailing waves affect both the gauge and calculation results. Fig. 10 illustrates this insight because a large wave height shows

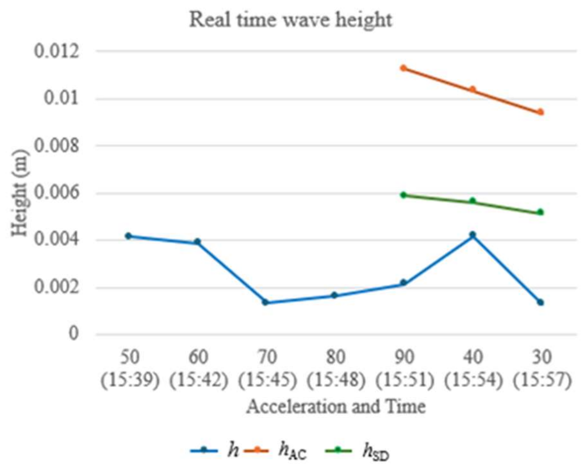

Fig. 12 Real-time wave height of high-acceleration (30%-90% of full acceleration) experiments.

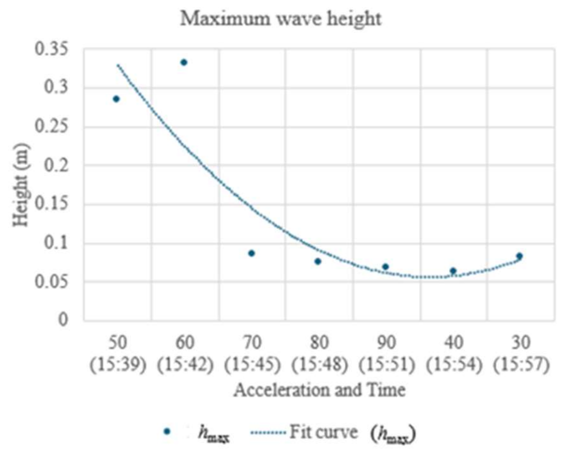

Fig. 13 Maximum wave height of high-acceleration (30%-90% of full acceleration) experiments.

increasing trends toward later points in experiments. Furthermore, during the low-acceleration experiment, under the same acceleration, the h experienced by the ship itself also exhibited different performance. In mid-acceleration and high-acceleration experiments, although the accelerations differed, no great difference was found in the h of the ship during the experiment, indicating that no clear relation exists between the ship's own speed and the wave height.

Small ships might face capsizing risks from lower wave heights than wave-height weather reports (statistically adjusted height: significant wave height) because h_{AC} and h_{SD} are statistically adjusted observations. Furthermore, they are always higher than h of the experiments.

In addition, although experiments were conducted in open areas, the waves generated by the ship model itself during navigation can affect its own motion state to some degree. This fact also suggests that other high-speed or large ships navigating nearby while the ship is sailing will generate navigation waves and will affect the h of nearby ships. In severe cases, such waves might cause capsizing accidents.

4. Conclusion

This study, using a series of experiments, investigated the wave response characteristics of a ship model under different motion conditions. After detecting the h received by the ship scale model through D3DCG and by calculating h_{max} to ascertain whether a risk of capsizing exists, this investigation compares and analyzes the wave height using D3DCG (h & h_{max}) along with the wave height detected by gauge (h_{AC} & h_{SD}). In practical situations, small ships might capsize because of waves with wave heights lower than those announced by government meteorological departments. The weather wave height released by the government is actually the wave height obtained through statistical analysis. It is the effective wave height obtained by integrating various actual wave heights; h_{SD} and h_{AC} are also wave heights obtained through statistical analysis. The fact that h is always lower than the statistical analysis wave height is quite severe because small and mid-sized ships such as passenger ships or fishing boats might capsize as a result of lower wave heights even when the statistical wave height reflects calm sea conditions.

Then, h_{max} is evaluated under different acceleration conditions. Regarding the analysis of h_{max}, it shows a trend of first decreasing and then increasing slightly. The ship model was able to withstand large wave heights at the beginning of the experiments. However, h_{max} decreased gradually as the experiment conditions changed, indicating that the ship model's wave resistance ability weakened at this stage. In the later stages of the experiment, h_{max} showed a certain degree of rebound, indicating that the ship model stability might be restored under specific motion conditions. In March 2026, a capsizing accident occurred in Okinawa [24]. The cause of the accident has not been fully determined, but from information reported by the media, it is speculated that the mechanism of this accident is consistent with the accident which occurred in Otsuma, Aomori, Japan [15]. At the time of the Okinawa accident, the wave height in the weather forecast was about 0.5 m, which is considered a calm sea condition for large cargo ships. However, h_{max} varies under different conditions. Therefore, it is speculated that in the accidents described above, h_{max} was very low. Consequently, even if the actual wave heights were lower than the reported wave heights, ship capsizing accidents still occurred. The research conclusions presented herein have referential importance for protecting the safety of small ships.

Overall, the experimentally obtained results revealed the wave response characteristics of the ship model under different motion conditions and verified the feasibility of the calculated results for trend prediction (e.g. sailing wave). Nevertheless, some deviation persists in wave height and amplitude prediction. Therefore, future research must use further optimized calculated results that have been calibrated with more experimentally obtained data to improve the wave height prediction accuracy and reliability. At the same time, in-depth research into *h* detection through ship motion is expected to be of great importance for protecting the navigation of small ships, and for improving ship stability assessment methods and maritime operation safety.

References

[1] Paulling, J. R., and Rosenberg, R. 1959. "On Unstable Ship Motions Resulting from Nonlinear Coupling." *Journal of Ship Research* 3 (2): 36-46.

[2] Thompson, J. 1997. "Designing against Capsize in Beam Seas: Recent Advances and New Insights." *Applied Mechanics Review* 50 (5). doi:10.1115/1.3101710.

[3] Spyrou, K., and Thompson, J. 2000. "The Nonlinear Dynamics of Ship Motions: A Field Overview and Some Recent Developments." *Philosophical Transactions of the Royal Society A* 358 (1771): 1735-60.

[4] Lee, Y. W., McCue, L., Obar, M., and Troesch, A. 2006. "Experimental and Numerical Investigation into the Effects of Initial Conditions on a Three Degree of Freedom Capsize Model." *Journal of Ship Research* 50 (1): 63-84.

[5] Papoulias, F. A. 1987. "Dynamic Analysis of Mooring Systems." Doctoral dissertation, Department of Naval Architecture and Marine Engineering, University of Michigan, Ann Arbor, MI.

[6] Falzarano, J. M. 1990. "Predicting Complicated Dynamics Leading to Vessel Capsizing." Doctoral dissertation, University of Michigan.

[7] Murashige, S., and Aihara, K. 1998. "Coexistence of Periodic Roll Motion and Chaotic One in a Forced Flooded Ship." *International Journal of Bifurcation and Chaos* 8 (3): 619-26.

[8] Murashige, S., and Aihara, K. 1998. "Experimental Study of Chaotic Motion of a Flooded Ship in Waves." *Proceedings of the Royal Society of London A* 454: 2537-53.

[9] Murashige, S., Yamada, T., and Aihara, K. 2000. "Nonlinear Analyses of Roll Motion of a Flooded Ship in Waves." *Philosophical Transactions of the Royal Society of London A* 358: 1793-812.

[10] Arnold, L., Chueshov, I., and Ochs, G. 2004. "Stability and Capsizing Ships in Random Sea—A Survey." *Nonlinear Dynamics* 36: 135-79.

[11] Spyrou, K. 1996. "Homoclinic Connections and Period Doublings of a Ship Advancing in Quartering Waves." *Chaos* 6: 95-107. https://doi.org/10.1063/1.166171.

[12] Kim, H., Haugen S., and Utne, I. B. 2015. "Assessment of Accident Theories for Major Accidents Particularly Addressing the MV SEWOL Disaster: Similarities, Differences, and Discussion for a Combined Approach." *Safety Science* 82: 410-20.

[13] Phoo, T., and Watanabe, Y. 2017. "Prevention of Ship Capsizing without Knowledge of Load or Hull Conditions." *Proceedings of the Fifth International Maritime-Port Technology and Development Conference* (MTEC 2017). ©2017 by MTEC 2017 Organizers. ISBN:978-981-11-2722-9. doi:10.3850/978-918-11-2722-9_MTEC020214.

[14] Kat, J. O. de. 1999. *Causes of Yacht Capsizing in Heavy Seas, Workshop on Safety of Ocean Racing Yachts, Sydney, Australia.* Accessed March 19, 1999.

[15] NHK. 2024. "Aomori: One of the Three Largest Tuna Fishermen Missing in a Fishing Boat Was Found to Be the First to Die for the First Time in the Race." Accessed December 20, 2024. https://news.ntv.co.jp/n/rab/category/society/ra0c11661742564b67943e53ae052a0bdc.

[16] Onodera, M., and Watanabe, Y. 2025. "Analysis of Maritime Accidents Based on Detection of Three-Dimensional Center of Gravity." Master thesis, Tokyo University of Marine Science and Technology, Tokyo, Japan.

[17] NHK. 2025. "Ibaraki: Fishing Boat Capsizes; Two Dead and Three Missing, Possibly Lost Balance Due to a Large Catch of Fish." Accessed February 1, 2025. https://www3.nhk.or.jp/shutokennews/20250106/1000112768.html.

[18] Pivert, F. L., Tizaoui, A., Alexandre, R., and Billard, J.-Y. 2017. "A Fully Analytical Method to Assess the Risk of Capsizing in Beam Sea." *Journal of Marine Science and Technology* 22: 125-34. doi:10.1007/s00773-016-0398-6.

[19] Watanabe, Y. 2017. 6131247 Patent No. of Japan, 2017.

[20] Watanabe, Y. 2017. 797724 Patent No. of USA, 2017.

[21] Watanabe, Y. 2017. ZL201380025549.X, Patent No. of China, 2017.

[22] Watanabe, Y. 2019. 10-2028231, Patent No. of Korea, 2019.

[23] Song, B. W. 2020. "Research on Capsizing Alert Based on Detecting the Three-Dimensional Center of Gravity." Master thesis, Tokyo University of Marine Science and Technology, Tokyo, Japan.

[24] NHK. 2026. "Capsizing Accident of a Protest Boat off Henoko Coast." Accessed March 23, 2026. https://www.yomiuri.co.jp/local/kyushu/news/20260323-GYS1T00007/.